

Assistive Control System for Upper Limb Rehabilitation Robot

Sung-Hua Chen, Wei-Ming Lien, Wei-Wen Wang, Guan-De Lee, Li-Chun Hsu, Kai-Wen Lee, Sheng-Yen

Lin, Chia-Hsun Lin, Li-Chen Fu, *Fellow, IEEE*, Jin-Shin Lai, Jer-Junn Luh, and Wen-Shiang Chen

Abstract—This paper presents an assistive control system with a special kinematic structure of an upper limb rehabilitation robot embedded with force/torque sensors. A dynamic human model integrated with sensing torque is used to simulate human interaction under three rehabilitation modes: active mode, assistive mode, and passive mode. The hereby proposed rehabilitation robot, called NTUH-ARM, provides 7 degree-of-freedom (DOF) motion and runs subject to an inherent mapping between the 7 DOFs of the robot arm and the 4 DOFs of the human arm. The Lyapunov theory is used to analyze the stability of the proposed controller design. Clinical trials have been conducted with 6 patients, one of which acts as a control. The results of these experiments are positive and STREAM assessment by physical therapists also reveals promising results.

Index Terms—Rehabilitation robotics, assistive control, upper extremity, exoskeleton.

I. INTRODUCTION

RECENT research has revealed that every year approximately 0.79 million people in the United States suffer from new or recurring strokes [1], the major symptoms of which are contracture and motor impairment. Several studies have demonstrated that repetitive functional motion is an effective therapeutic treatment for stroke patients, positively influencing their degree of recovery [2]. The key factors involved in successful therapy are task-specific training [3], high intensity and duration [2], repetitive training [4], the active participation of the patient [5], and maximal challenge [5].

Compared with traditional rehabilitative therapy, robot-aided rehabilitation can increase the intensity of therapy, reduce the workload of medical staff, and provide a quantitative record with regard to the progress of recovery. Furthermore, robotic devices combined with games played in virtual reality can increase the motivation of patients to participate in task-oriented rehabilitation. MIT Manus [6], Mirror Image Motion Enabler [7], and GENTLE/s [8] are all examples of

robot-oriented rehabilitation devices of the end-effector form. This study proposes the use of an exoskeleton arm, the advantages of which include increased ability to assess individual joint angles in the human arm in a precisely defined manner. The pre-determined profile of the robot arm posture lends itself better to the control of individual joints. The adverse effect of synergy patterns caused by end-effector robots can also be reduced, thereby improving the ability to coordinate various movements associated with the upper limbs. Furthermore, the interactive torques exerted from specific joints can be analyzed more easily using an exoskeleton robot arm. For instance, a musculoskeletal model has been integrated with the Assist-As-Needed (AAN) control strategy by considering factors such as limb pose, direction of external force, and muscular impairment [9]. Finally, compared with the end-effector robot, the exoskeleton robot has larger range of motion (ROM), enabling movement more imitative of the motions required in daily life. ARMin I, II and III [10-12], MGA Exoskeleton [13], IntelliArm [14], L-Exos [15], and the NTUH-ARM [16] are examples of robots based on an exoskeleton design. Generally, there are two strategies to achieve active-assistive range of motion (A-AROM). One is to amplify the human torque, such as [22, 23], whereas the other is to adopt the assist-as-needed strategy like [24, 25]. The former strategy enlarges the robot's assistance to help patients lacking power to proceed the motion task further, while the later strategy designed an algorithm to provide a robotic support only when patient cannot keep up with the reference training motion.

Different from other studies, the proposed assistive mode in this research derives the desired motion trajectories with the help from human arm dynamics. This desired motion can be viewed as the ideal human motion. In addition, to provide a reasonable assistance in the proposed AAN strategy, we define a smooth motion trajectory as basis to determine the timing to switch on/off the assistance. This mechanism let the robot support the patients only when the patients fall behind the desired trajectories. Several real clinical tests are conducted to further validate this control design have actual efficacy for patient's motor function recovery.

The remainder of this paper is organized as follows. The hardware design of a 7-DOF exoskeleton-type rehabilitation robot, the National Taiwan University Hospital-ARM (NTUH-ARM), is introduced in Section II. The joint mapping between various joints of the robot arm and shoulder/elbow joints of the human arm, as well as the control strategies are

This work was supported in part by National Science Council, R.O.C., via contracts: NSC 104-2627-E-002-006.

S.-H. Chen, W.-M. Lien, W.-W. Wang, G.-D. Lee, L.-C. Hsu, K.-W. Lee, S.-Y. Lin, and C.-H. Lin are with the Department of Electrical Engineering, National Taiwan University, Taiwan, R.O.C.

L.-C. Fu is with the Department of Electrical Engineering and Department of Computer Science and Information Engineering, National Taiwan University, Taiwan, ROC (e-mail: lichen@ntu.edu.tw).

J.-S. Lai, J.-J. Luh, and W.-S. Chen are with the Department of Physical Medicine and Rehabilitation, National Taiwan University (NTU) and NTU Hospital, R.O.C. (e-mail: jslai@ntu.edu.tw).

presented in Section III. Stability of the control strategy is evaluated in Section IV. Several experiments and results demonstrating the effectiveness of the proposed assistive controller and its advantages are included in Section V. Finally, conclusions are drawn in Section VI.

II. METHODOLOGY

A. Kinematic Design

In designing the NTUH-ARM (Fig. 1), the objective is to produce appropriate recovery trajectories for the joints of a patient suffering the effects of stroke. The NTUH-ARM has 7 DOFs, in which the first six DOFs correspond to the shoulder joint (including one prismatic joint and five rotational joints), and the last corresponds to the elbow joint (Fig. 2). Such mapping relationship between robotic joints to human movement is due to intrinsic mechanical design of NTUH-ARM. Through this redundant design for joint alignment, NTUH-ARM is able to allow the patient to achieve five movements for the shoulder joint (shoulder adduction/abduction, shoulder flexion/extension, shoulder internal/external rotation, elevation/depression, and protraction/retraction) and one movement for elbow joint (elbow flexion/extension). Furthermore, there are another three main reasons for using a high-DOF design for the shoulder joint: 1) avoiding singularity in the reachable workspace, 2) increasing the ROM of the shoulder joint, and 3) dealing with the displacement of the glenohumeral-joint (GH-joint) [17] by preprogramming the trajectory of the GH-joint. Fig. 3 shows the kinematic structure of the developed NTUH-ARM based on the Denavit-Hartenberg (D-H) model; corresponding parameters are given in Table I. The lengths of the upper arm (26~34cm) and the forearm (24~30cm) are passively adjustable to suit the patient [16].

B. Hardware Configuration and Interface

From a mechanical perspective, the NTUH-ARM uses

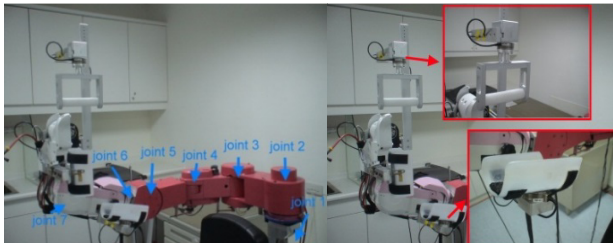


Fig. 1 Mechanical structure and DOF distribution of NTUH-ARM (NTUH: National Taiwan University Hospital). Two 6-axis force/torque sensors are used to measure the force of interactions between the patient's arm and the robot arm. One is equipped on the splint of the upper arm; the other is mounted on the wrist gripper.

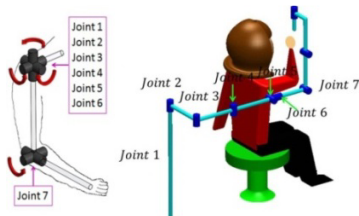


Fig. 2 Association of motion between human upper limb and NTUH-ARM

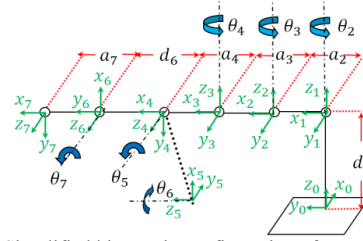


Fig. 3 Simplified kinematic configuration of NTUH-ARM

Table I. DENAVIT–HARTENBURG PARAMETERS OF NTUH-ARM

Axis	θ_i	d_i	a_i	α_i	Home
1	0	d_1	0	0	$\pi/2$
2	θ_2	0	a_2	0	0
3	θ_3	0	a_3	0	0
4	θ_4	0	a_4	$-\pi/2$	0
5	θ_5	0	0	$-\pi/2$	$-\pi/2$
6	θ_6	d_6	0	$\pi/2$	0
7	θ_7	0	a_7	0	$\pi/2$

brushed FAULHABER DC motors to incorporate the harmonic drives on every joint to increase the torque associated with joint actuators. In contrast to previous designs [16], two sensitive 6-axis force/torque (F/T) sensors are mounted at the upper arm and front of the wrist handle to measure the interaction F/T feedback (Fig. 1). At each joint, a potentiometer and encoder are used to measure the joint position. Using these two kinds of position sensors enables the robot to analyze and record the position of each joint for any configuration of the upper arm. The potentiometer can also be used to set the initial position of the robot. In addition, we used the NI USB-6229 Data Acquisition device to acquire analog signals from sensors and LabVIEW to develop the proposed control software. The hardware configuration of the system is presented in Fig. 4. Two emergency stop buttons are also provided: one attached to the control panel and the other configured as a portable hand-button that can be held by either the patient or therapist.

The user interface developed with LabVIEW provides the function of trajectory settings with which the therapist may generate or edit the personal arm trajectories of patients. These trajectories can be established by defined angle and ROM based on the time domain. The therapist can adjust type of movement and speed according to control capacity exhibited by each patient. In addition, the therapist can set multiple joints in motion simultaneously. The settings of trajectory will be saved in the database for repetitive use. A trajectory exceeding the set speed limit will produce an error notification and the invalid trajectory will not be released for rehabilitation use.

III. ASSISTIVE CONTROL SYSTEM

The assistive control system is meant to help patients exercise their limbs to their maximum ability. Fig. 5 presents a control block diagram of the overall system. The Robot-to-Human Joint-Mapping block of the robot arm receives the angles of the various robot joints and transforms them into the angles of human joints through specific geometric relationships. The Gravity Compensation block removes the influence of gravity from the human torque exertion so that the measured torques from the F/T sensors will be free of gravity.

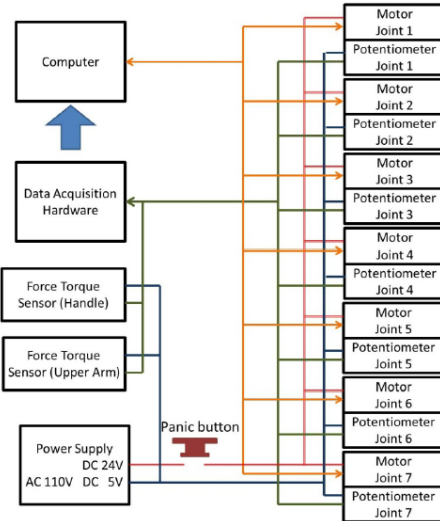


Fig. 4 Block diagram of hardware configuration

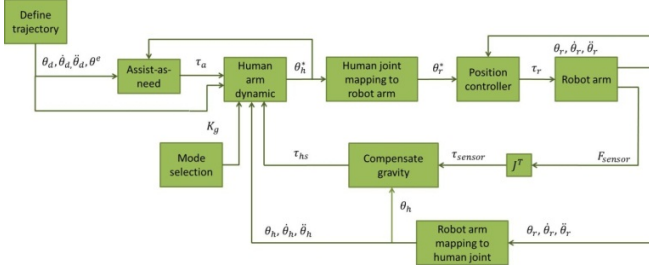


Fig. 5 Control block diagram

The Define Trajectory block outputs trajectories designed by therapists. The AAN Strategy block helps to compare the difference between the defined motion trajectory and the current human joint motion. The Mode Selection block allows therapists to choose the gain to amplify the motion torques generated by the patient and rehabilitation modes. The Human Arm-Dynamics block simulates human arm movements. The Human-to-Robot Joint-Mapping block derives each corresponding robot joint angle from the human joint angles through direct and inverse kinematics. Further details are described in our previous works [16, 18].

The kinematic model of the human upper extremity can be represented using a D-H parametric model as demonstrated in Fig. 6 where joints 1, 2, and 3 together represent the shoulder joint respectively producing the shoulder's horizontal adduction/ abduction, flexion/extension, and internal/external rotation. It is worth mentioning that these three joints intersecting at one point act as a ball and socket joint. Besides, for simplicity of proposed AAN therapy, we only considered rotational joints which correspond to shoulder adduction/abduction, shoulder flexion/extension, and shoulder internal/external rotation movement. Therefore, only 3 DOFs in the shoulder are used when modeling kinematic of human upper extremity, and the remaining 2 DOFs of human shoulder joints for elevation/depression and protraction /retraction are not consider in the framework of AAN. Joint 4 indicates the motion of elbow flexion/extension. L_u and L_f are the lengths of the upper arm and forearm, respectively. The human arm's D-H parameters are presented in Table II.

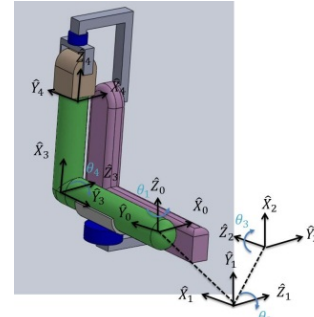


Fig. 6 Kinematic model of human upper extremity.

Table II. DENAVIT–HARTENBURG PARAMETERS OF THE HUMAN ARM

Axis	θ_i	d_i	a_i	α_i	Home
1	$\theta_{h,sh}$	0	0	$\pi/2$	$\pi/2$
2	$\theta_{h,sv}$	0	0	$\pi/2$	$\pi/2$
3	$\theta_{h,sr}$	L_u	0	$-\pi/2$	0
4	$\theta_{h,e}$	0	L_f	$-\pi/2$	$-\pi/2$

A. Robot-to-Human Joint Mapping

The kinematic structure of the robot arm (as demonstrated in Fig. 7) establishes specific geometric relationships between the human arm posture and the robot arm configuration, allowing the mapping of robot joint angles onto human joint angles. In the following we present the mapping for human elbow flexion/extension $\theta_{h,e}$, shoulder flexion/extension $\theta_{h,sv}$, shoulder horizontal adduction/abduction $\theta_{h,sh}$, and shoulder internal/external rotation $\theta_{h,sr}$ from various robot joints $\theta_{r,k}$, where k is the k th robot joint angle, and $k=2,\dots,7$:

$$\begin{aligned} \theta_{h,e} &= -\theta_{r,7} \\ \theta_{h,sv} &= -\theta_{r,5} \\ \theta_{h,sh} &= \theta_{r,2} + \theta_{r,3} + \theta_{r,4} - \frac{\pi}{2} \\ \theta_{h,sr} &= \theta_{r,6} \end{aligned} \quad (1).$$

(1) enables the mapping of robot joint angles to the angles of human arm joints. We can also use finite difference approximation to obtain a reasonably accurate value for the angular velocity of a human arm joint.

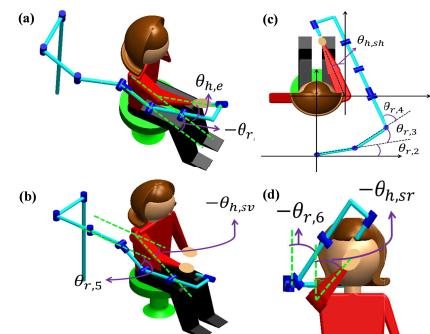


Fig. 7 Relationship between the robot arm and the human arm: (a) elbow flexion/extension; (b) shoulder flexion/extension; (c) shoulder horizontal adduction/abduction; and (d) shoulder internal/external rotation

B. Human-to-Robot Joint Mapping

From Fig. and Table II, we can easily derive the forward kinematics of the human arm. The positions of the human joints can be mapped to the robot joint locations as demonstrated in

Fig. 8, from which the corresponding robot joint angles can be derived using the inverse kinematics of the robot [16].

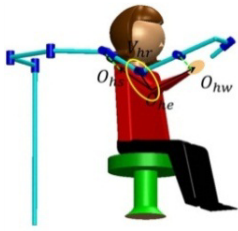


Fig. 8 Relationship between positions of various joints of the robot arm and positions of the human shoulder, elbow, and wrist joints: vector V_{hr} is defined as the normal vector of the plane containing the three joint positions of the human arm

C. Analyzing Joint Torque from Measurement Sensor

Referring to the configuration of the NTUH-ARM as demonstrated in Fig. 10, the force and torque sensors are mounted on the upper arm and the gripper, respectively. The idea of this placement is to allow the sensing of the torques generated from the human arm joints by the F/T sensors. Moreover, this measured torque is treated as the main input parameter to control the robot. The procedure of analyzing the joint torques extracted by the measurement sensors is as follows. First we use the force-moment transformation to transform the torque measured from the two sensors into the same frame, as illustrated in Fig. 9.

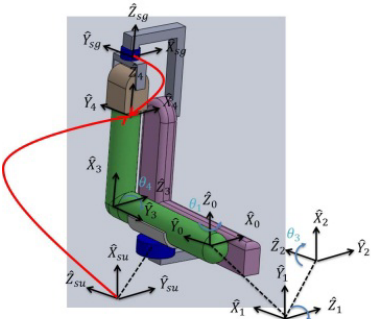


Fig. 9 Measured force/torque from each sensor transferred to the wrist frame (frame {4})

The force-moment transformation formula is as follows:

$$\begin{bmatrix} {}^2f_{2,su} \\ {}^2n_{2,su} \end{bmatrix} = \begin{bmatrix} {}^{su}R & 0 \\ {}^2P_{su,org} \times {}^{su}R & {}^{su}R \end{bmatrix} \begin{bmatrix} {}^{su}f_{su} \\ {}^{su}n_{su} \end{bmatrix} \quad (2)$$

where

- ${}^{su}f_{su}$ is a 3×1 force vector measured from the upper arm's F/T sensor described in frame {su} (also corresponding to the force exerted on the human upper arm)
- ${}^{su}n_{su}$ is a 3×1 moment vector measured from the upper arm's F/T sensor described in frame {su} (also corresponding to the torque exerted on the human upper arm)
- ${}^{su}R$ is a rotation matrix describing the orientation of frame {su} relative to frame {2}
- ${}^2P_{su,org}$ is a 3×1 vector pointing from the origin of frame {su} to that of frame {2} represented in frame {2}
- ${}^2f_{2,su}$ is a 3×1 force vector showing the force exerted on the human upper arm represented in frame {2}
- ${}^2n_{2,su}$ is a 3×1 moment vector showing the moment exerted on the human upper arm represented in frame {2}.

Then, we transform the forces and moments represented in frame {2} into those represented in frame {4} as follows:

$$\begin{bmatrix} {}^4f_{4,su} \\ {}^4n_{4,su} \end{bmatrix} = \begin{bmatrix} {}^4R & 0 \\ {}^4P_{2,org} \times {}^4R & {}^4R \end{bmatrix} \begin{bmatrix} {}^2f_{2,su} \\ {}^2n_{2,su} \end{bmatrix} \quad (3)$$

where

- 4R is a rotation matrix describing the orientation of frame {2} relative to frame {4}
- ${}^4P_{2,org}$ is a 3×1 vector locating the origin of frame {2} relative to frame {4}
- ${}^4f_{4,su}$ is a 3×1 force vector showing the force exerted on the human upper arm described in frame {4}
- ${}^4n_{4,su}$ is a 3×1 moment vector showing the moment exerted on the human upper arm described in frame {4}.

Note that here the two 3×1 vectors ${}^2P_{su,org}$ and ${}^4P_{2,org}$ are expanded into the 3×3 skew-symmetric matrices.

Similarly, we can obtain the F/T measurement in frame {4} from the gripper's force/moment sensor frame {sg}. We combine data from the sensor units in the upper arm and the gripper in frame {4}, as follows:

$$\begin{bmatrix} {}^4f_{4,total} \\ {}^4n_{4,total} \end{bmatrix} = \begin{bmatrix} {}^4f_{4,su} \\ {}^4n_{4,su} \end{bmatrix} + \begin{bmatrix} {}^4f_{4,sg} \\ {}^4n_{4,sg} \end{bmatrix} \quad (4)$$

where

- ${}^4f_{4,total}$ is the 3×1 total force vector described in frame {4}, indicating the sum of a force exerted on the upper arm and a force exerted on the gripper
- ${}^4n_{4,total}$ is the 3×1 total moment vector described in frame {4}, indicating the sum of a moment exerted on the upper arm and a moment exerted on the gripper
- ${}^4f_{4,sg}$ is a 3×1 force vector showing the force exerted on the gripper described in frame {4}
- ${}^4n_{4,sg}$ is a 3×1 moment vector showing the moment exerted on the gripper described in frame {4}.

After combining these two forces and two moment vectors, the Jacobian transpose can be used to map the summed Cartesian generalized forces into various human joint torques (Fig. 50). Specifically, the Cartesian force ${}^4f_{4,total}$ and moment ${}^4n_{4,total}$ in frame {4} are mapped into the equivalent human joint torques through Jacobian transpose:

$$\tau_{h,sensor} = {}^4J_{4,h}^T \begin{bmatrix} {}^4f_{4,total} \\ {}^4n_{4,total} \end{bmatrix} \quad (5)$$

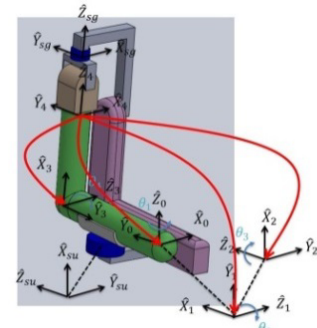


Fig. 50 Jacobian transpose mapping total force/moment with respect to the human wrist frame in Cartesian space into torques at various human joints in joint space

where

- ${}^4J_{4,h}^T$ is the Jacobian transpose of the human upper extremity described in frame {4}
- $\tau_{h,sensor}$ is a vector of human joint torques derived from the sensor measurements.

D. Model of Human Arm Dynamics

Regarding the human upper extremity as a manipulator, we can derive the free-motion human arm dynamics model from the Lagrange approach as follows:

$$\tau_{hm} = M_h(\theta_h)\ddot{\theta}_h + V_h(\theta_h, \dot{\theta}_h) + G_h(\theta_h) + F_h(\theta_h, \dot{\theta}_h) \quad (6)$$

where

- θ_h , $\dot{\theta}_h$, and $\ddot{\theta}_h$ are the vector of human joint angles, joint angular velocities, and joint angular accelerations
- τ_{hm} is a 4×1 vector of motion torques generated from the patient
- $M_h(\theta_h)$ is the inertia matrix
- $V_h(\theta_h, \dot{\theta}_h)$ is the vector of centrifugal and Coriolis terms
- $G_h(\theta_h)$ is the gravity vector
- $F_h(\theta_h, \dot{\theta}_h)$ is the friction vector of the upper limb.

The dynamic model is calculated based on an existing human database. For instance, we employed a cylinder to model each segment of the human upper limb (i.e., upper arm or forearm) [19], and then took the center of mass of each segment from the literature [20]. Assuming the human arm and robot arm connected during the motion, the difference in velocity between them can be disregarded. Thus, we can obtain the following equation:

$$\tau_{hm} = J^T F_{hm} = J^T F_{sensor} \quad (7)$$

where

- F_{hm} is the human arm Cartesian force from human to robot
- F_{sensor} is the Cartesian force sensing from robot

Note that F_{sensor} can be measured by the F/T sensor. By combining (6) and (7), and replacing the motion torque with the measured sensor torque $J^T F_{sensor}$, we can obtain the dynamic equation as follows:

$$J^T F_{sensor} = M_h(\theta_h)\ddot{\theta}_h + V_h(\theta_h, \dot{\theta}_h) + G_h(\theta_h) + F_h(\theta_h, \dot{\theta}_h) \quad (8)$$

To simulate the motion of the human arm using human joint acceleration, we reform (8) as

$$\ddot{\theta}_h = M_h^{-1}(\theta_h)[J^T F_{sensor} - G_h(\theta_h) - V_h(\theta_h, \dot{\theta}_h) - F_h(\theta_h, \dot{\theta}_h)] \quad (9)$$

In order to achieve the assistive mode (torque amplification), we combine the $J^T F_{sensor}$ and $G_h(\theta_h)$ to achieve gravity compensation, where the ideal motion model is as follows:

$$\ddot{\theta}_h^* = M_h^{-1}(\theta_h)[K_g \tau_{hs} - V_h(\theta_h, \dot{\theta}_h) - F_h(\theta_h, \dot{\theta}_h)] \quad (10)$$

with the following notations:

- $\ddot{\theta}_h^*$: angular accelerations of the target motion of the human upper limb
- τ_{hs} : vector of measured human torque exerted after gravity compensation (for performing the target motion)
- K_g : diagonal gain matrix to adjust effective torque exhibited at each joint

$$K_g = \begin{bmatrix} k_{sh} & 0 & 0 & 0 \\ 0 & k_{sv} & 0 & 0 \\ 0 & 0 & k_{sr} & 0 \\ 0 & 0 & 0 & k_e \end{bmatrix} \quad (11)$$

- k_{sh} : gain for the horizontal adduction/ abduction of the shoulder
- k_{sv} : gain for the flexion/extension of the shoulder
- k_{sr} : gain for internal/external rotation of the shoulder
- k_e : gain for the flexion/extension of the elbow.

E. Define Trajectory

To implement the AAN strategy, therapists must define a desired trajectory for patients to follow. To create a smooth trajectory with continuous positioning and velocity, this study used the cubic spline method. The form of the cubic polynomial for the i th joint of the human arm is as follows:

$$\theta_{di}(t) = a_0 + a_1 t + a_2 t^2 + a_3 t^3 \quad (12)$$

resulting in the corresponding velocity and acceleration:

$$\dot{\theta}_{di}(t) = a_1 + 2a_2 t + 3a_3 t^2 \quad (13)$$

$$\ddot{\theta}_{di}(t) = 2a_2 + 6a_3 t \quad (14)$$

where $\theta_{di}(t)$, $\dot{\theta}_{di}(t)$, and $\ddot{\theta}_{di}(t)$ are respectively the angle, angular velocity, and angular acceleration of the i th joint in the defined trajectory, and a_0 , a_1 , a_2 , and a_3 represent appropriate parameters of the polynomial. Next, by identifying the relevant control via points, between the j th and the $(j+1)$ th via points, the following relationships can be used to describe the movement of i th joint:

$$\theta_{dij} = a_{0ij} \quad (15)$$

$$\theta_{di(j+1)} = a_{0ij} + a_{1ij} t_{j+1} + a_{2ij} t_{j+1}^2 + a_{3ij} t_{j+1}^3 \quad (16)$$

$$\dot{\theta}_{dij} = a_{1ij} \quad (17)$$

$$\dot{\theta}_{di(j+1)} = a_{1ij} + 2a_{2ij} t_{j+1} + 3a_{3ij} t_{j+1}^2 \quad (18)$$

where θ_{dij} and $\dot{\theta}_{dij}$ are the angle and angular velocity of the i th joint at the j th via point; $\theta_{di(j+1)}$ and $\dot{\theta}_{di(j+1)}$ are angle and angular velocity of the i th joint at the $(j+1)$ th via point; t_{j+1} is the time elapsed between the j th point and $(j+1)$ th point, and a_{0ij} , a_{1ij} , a_{2ij} , and a_{3ij} represent the parameters of the cubic polynomial at the i th joint between the j th via point and the $(j+1)$ th via point.

F. Assist-as-Needed

After the trajectory has been defined, it is necessary to generate torque at appropriate times in order to support the patient to move his/her arm to follow the trajectory successfully. The torque generated from the i th joint trajectory is demonstrated as follows ($i=1\sim 4$):

$$\tau_{ai}(t) = m_{aii}\ddot{\theta}_{di}(t) + m_{aii}(\theta_{di}(t) - \theta_{hi}^*(t)) + 2m_{aii}(\dot{\theta}_{di}(t) - \dot{\theta}_{hi}^*(t)) \quad (19)$$

where

- $\theta_{di}(t)$, $\dot{\theta}_{di}(t)$, and $\ddot{\theta}_{di}(t)$ are the angle, angular velocity, and angular acceleration of the i th joint throughout the defined trajectory;
- $\theta_{hi}^*(t)$ and $\dot{\theta}_{hi}^*(t)$ are the target angle and angular velocity of the i th joint;
- $\tau_{ai}(t)$ is the AAN torque of the i th joint;
- m_{aii} is a positive constant.

Let

$$\tau_a(t) = \begin{bmatrix} \tau_{a1}(t) \\ \tau_{a2}(t) \\ \tau_{a3}(t) \\ \tau_{a4}(t) \end{bmatrix} \quad (20)$$

Substituting (20) into (10) enables the modification of the ideal motion model with assistive torque to achieve our AAN goal, as follows:

$$\ddot{\theta}_h^* = (I - K_s)M_h^{-1}(\theta_h)[K_g\tau_{hs} - V_h(\theta_h, \dot{\theta}_h) - F_h(\theta_h, \dot{\theta}_h)] + K_s M_a^{-1}\tau_a \quad (21)$$

where

- M_a is the following diagonal positive definite matrix

$$M_a = \begin{bmatrix} m_{a11} & 0 & 0 & 0 \\ 0 & m_{a22} & 0 & 0 \\ 0 & 0 & m_{a33} & 0 \\ 0 & 0 & 0 & m_{a44} \end{bmatrix} \quad (22)$$

- K_s is the following diagonal matrix for switching τ_a

$$K_s = \begin{bmatrix} k_{s1} & 0 & 0 & 0 \\ 0 & k_{s2} & 0 & 0 \\ 0 & 0 & k_{s3} & 0 \\ 0 & 0 & 0 & k_{s4} \end{bmatrix} \quad (23)$$

$$k_{si} = \begin{cases} 1 & \dot{\theta}_{hi}(t)(\theta_{di}(t) - \theta_{hi}(t)) > 0 \\ 0 & \text{otherwise} \end{cases} \quad (24)$$

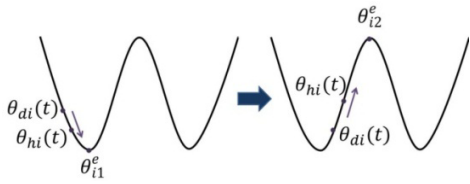


Fig. 61 Relationship between human joint angle, defined trajectory angle, and extreme angle

As demonstrated in Fig. 61, θ_{ij}^e represents the i th joint angle at the j th extreme point, where $i = 1 \sim 4$, and $j = 1, 2, \dots, n$. Let $\theta_{di}(t) = \theta_{ij}^e$ when $t = t_j$, then given $\theta_{hi}(t)$ and $\dot{\theta}_{hi}(t)$, assessing the switching criterion described in (24) should be straightforward. With this assistance condition, the robot will support the patient in moving along a predefined trajectory only if the patient moves slower than the defined trajectory. Otherwise, the patient will have to move by himself/herself in active mode. In other words, the robot will assist the patient only as he/she requires assistance.

After obtaining the target angular acceleration from (21), we can then calculate the joint angles and angular velocities through Euler integration. According to (21), the device can operate in active mode when K_g equals I and K_s is 0; if k_{sh}, k_{sv}, k_{sr} , or k_e is greater than 1 and K_s is 0, the assistive mode (torque amplification) will be selected; otherwise, if K_g is equal to I and k_{si} is equal to 1, assistive mode will be selected. Furthermore, when K_g is 0 and K_s is equal to I , the robot will operate in passive mode. Table III summarizes the conditions of each rehabilitative mode.

Passive mode provides total support to stroke patients who cannot exercise voluntarily. Active mode is used by patients with mild disability and sufficient muscle strength with a focus on enhancing motor learning and helping brain lesions to re-organize. Assistive mode moves between these two modes,

providing assistance or resistance according to the motor abilities of the patient.

Table III. REHABILITATION MODE

Rehabilitation mode	Active	Assistive	Passive
Coefficient	$K_g = I, K_s = 0$	$k_{sh}, k_{sv}, k_{sr}, \text{ or } k_e > 1, K_s = 0$ or $K_g = I, K_s = I$	$K_g = 0, K_s = I$

IV. STABILITY ANALYSIS

This section demonstrates the stability of the proposed assistive control system. First, we show that the assistive torque (generated from the relationship between defined trajectory θ_d and target human trajectory θ_h^*) leads to $\theta_h^* \rightarrow \theta_d$ and $\dot{\theta}_h^* \rightarrow \dot{\theta}_d$. Second, we show that the actual proposed robot joint angles are driven to the desired setting.

In the previous section, we stated that the assistive torque generated from the defined trajectory described in (19), will support patients. We will now present a description of this process. In the assistive mode, (21) becomes

$$\ddot{\theta}_{hi}^* = m_{ai}^{-1}\tau_{ai} \quad (25)$$

Let angle error $e_1 = \theta_{di} - \theta_{hi}^*$ and angular velocity error $e_2 = \dot{\theta}_{di} - \dot{\theta}_{hi}^*$, and use these to define a Lyapunov function candidate V_a which takes the form of the following positive definite function:

$$V_a = \frac{1}{2}(e_1 + e_2)^T(e_1 + e_2) \quad (26)$$

The time derivative of the function is obtained as follows:

$$\begin{aligned} \dot{V}_a &= (e_1 + e_2)^T(\dot{e}_1 + \dot{e}_2) \\ &= (e_1 + e_2)^T(e_2 + \dot{e}_2) \\ &= (e_1 + e_2)^T(e_2 + \ddot{\theta}_{di} - m_{ai}^{-1}\tau_{ai}) \end{aligned} \quad (27)$$

Substituting τ_{ai} into (27) results in

$$\dot{V}_a = -(e_1 + e_2)^T(e_1 + e_2) \leq 0 \quad (28)$$

If $\dot{V}_a = 0$, then either (i) $e_1 = 0, e_2 = 0$, or (ii) $e_1 + e_2 = 0$. In case (ii),

$$e_2 = -e_1 \quad (29)$$

$$\dot{e}_1 = -\dot{e}_1 \quad (30)$$

which ensures $e_1 \rightarrow 0$ and $e_2 \rightarrow 0$ as time t approaches infinity; in other words, we demonstrate $\theta_{hi}^* \rightarrow \theta_{di}$ and $\dot{\theta}_{hi}^* \rightarrow \dot{\theta}_{di}$ when patients require support from the robot.

We must therefore prove that the actual angles of the robot joints will match those desired. The general form of the dynamic equation of the robot arm system can be expressed as

$$\begin{aligned} \tau_r &= M_r(\theta_r)\ddot{\theta}_r + V_r(\theta_r, \dot{\theta}_r) + G_r(\theta_r) + F_r(\theta_r, \dot{\theta}_r) \\ &\quad + \tau_{dis} - \tau_{int} \end{aligned} \quad (31)$$

with the notations given below:

- $\theta_r, \dot{\theta}_r, \ddot{\theta}_r$: vector of the robot joint angles, joint angular velocity, and joint angular acceleration
- τ_r : robot joint torques
- $M_r(\theta_r)$: inertia matrix of the robot arm
- $V_r(\theta_r, \dot{\theta}_r)$: centrifugal and Coriolis of the robot arm
- $G_r(\theta_r)$: gravity of the robot arm
- $F_r(\theta_r, \dot{\theta}_r)$: friction of the robot arm

- τ_{dis} : disturbance torques or un-modeled dynamics of the rehabilitation robotic system
- τ_{int} : interaction torque between human arm and robot arm.

We define the required joint torques of the robot arm as follows:

$$\begin{aligned}\tau_r = M_r(\theta_r)\ddot{\theta}_r^* + M_r(\theta_r)u + V_r(\theta_r, \dot{\theta}_r) \\ + G_r(\theta_r) + F_r(\theta_r, \dot{\theta}_r) - \tau_{int}\end{aligned}\quad (32)$$

where $\ddot{\theta}_r^*$ is the target angular acceleration of the robot arm, and u is a control input. Equating (31) and (32), we obtain

$$M_r(\theta_r)\ddot{\theta}_r + \tau_{dis} = M_r(\theta_r)\ddot{\theta}_r^* + M_r(\theta_r)u \quad (33)$$

Let angle error $e_{r1} = \theta_r^* - \theta_r$, angular velocity error $e_{r2} = \dot{\theta}_r^* - \dot{\theta}_r$, and $\xi = M_r^{-1}(\theta_r)\tau_{dis}$ have the upper bound $\rho > |M_r^{-1}(\theta_r)\tau_{dis}|$. Thus, (33) becomes

$$\dot{e}_{r2} = \xi - u \quad (34)$$

Input u is defined as follows:

$$u = e_{r2} + \rho \text{sgn}(e_{r1} + e_{r2}) \quad (35)$$

Substituting u into (34) we obtain

$$\dot{e}_{r2} = \xi - e_{r2} - \rho \text{sgn}(e_{r1} + e_{r2}) \quad (36)$$

If we define a Lyapunov function candidate V_r as follows

$$V_r = \frac{1}{2}(e_{r1} + e_{r2})^T(e_{r1} + e_{r2}) \quad (37)$$

then the time derivative of the function is

$$\begin{aligned}\dot{V}_r &= (e_{r1} + e_{r2})^T(\dot{e}_{r1} + \dot{e}_{r2}) \\ &= (e_{r1} + e_{r2})^T(e_{r2} + \dot{e}_{r2}) \\ &= (e_{r1} + e_{r2})^T[\xi - \rho \text{sgn}(e_{r1} + e_{r2})] \\ &= (e_{r1} + e_{r2})^T\xi - \rho(e_{r1} + e_{r2})^T \text{sgn}(e_{r1} + e_{r2}) \\ &= (e_{r1} + e_{r2})^T\xi - \rho \sum_i |e_{r1i} + e_{r2i}| \\ &\leq |e_{r1} + e_{r2}| |\xi| - \rho \sum_i |e_{r1i} + e_{r2i}| < 0\end{aligned}\quad (38)$$

Here, $V_r < 0$ means, as time t approaches infinity, $e_{r1} + e_{r2} \rightarrow 0$, which ensures $e_{r1} \rightarrow 0$ and $e_{r2} \rightarrow 0$; in other words, we have demonstrated $\theta_r \rightarrow \theta_r^*$ and $\dot{\theta}_r \rightarrow \dot{\theta}_r^*$. Next, we can use structural conditions and geometric relationships that map the robot joint angles to the human joint angles, and vice versa. Therefore, $\theta_r \rightarrow \theta_r^*$ and $\dot{\theta}_r \rightarrow \dot{\theta}_r^*$ means that $\theta_h \rightarrow \theta_h^*$ and $\dot{\theta}_h \rightarrow \dot{\theta}_h^*$. This guarantees that the proposed assistive system is capable of operating in all selected rehabilitation modes.

V. EXPERIMENTS AND RESULTS

This section presents the experiments and clinical tests performed to validate the proposed system. In the first part, we demonstrate the tracking performance of the robot in passive mode to validate the controller. The second part shows the results of gravity compensation mentioned in Section III, and then represents the comparison of active and assistive mode with a window-cleaning game. To validate the efficiency of proposed AAN control strategy, in the subsequent experiments, we inspect each phases of the assistive mode in one exercise cycle. The last part shows the clinical tests which were conducted with six participants. The frequency domain analyses are also provided to verify the smoothness of the motion.

A. Passive mode

Fig. 12 shows the flexion/extension of the elbow in passive mode (right) and internal/external rotation of the shoulder (left)

related to the generated trajectory. The first graphs show the predefined angle of trajectory; the second two display the measured angle profile; and the bottom graphs present the error between the predefined angle trajectory and measured angle profile. The root mean square error values of the elbow and shoulder are 1.04° and 0.3° , respectively. The tracking performance in passive mode verified the controller's effect.

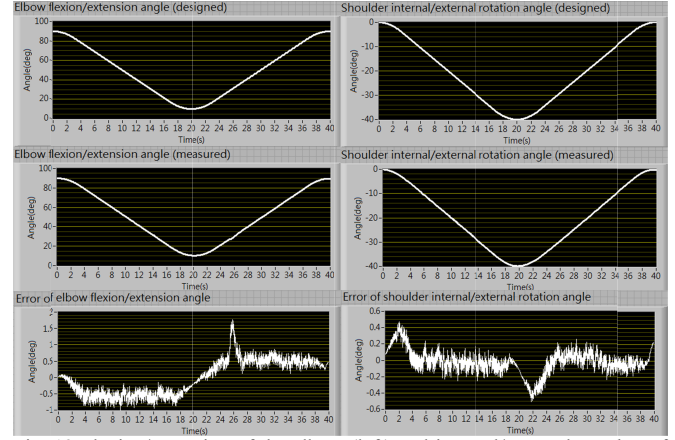


Fig. 12 Flexion/extension of the elbow (left) and internal/external rotation of the shoulder (right) in passive mode

B. Active and assistive modes

In active and assistive modes, the gravity-compensated controller described in the control block diagram (Fig. 6) can eliminate the influence of gravity, and thus enables the analysis of joint torque in the therapy.

We now present the results of the window-cleaning game [21] in active mode ($k_{sh} = 1$, and $k_{sv} = 1$) and assistive mode ($k_{sh} = 1.3$, and $k_{sv} = 1.3$). In this game, patients are asked to clean a virtual window by moving their arms in a clockwise spiral from the outer edges to the center of the window, thereby enabling a detailed assessment of current motor control. Fig. 13 shows the end-point (hand) trajectory in 2-D space. This movement requires 2-DOF motion: shoulder flexion/extension, and horizontal adduction/abduction of the shoulder. In both modes, the patient attempts to finish the game in approximately 40 seconds. Fig. 14 and Fig. 15 provide sample results from the game. Torque exerted by the patient in active mode (Fig. 14: the top row shows angles of $-35^\circ \sim 0^\circ$ and $-30^\circ \sim 0^\circ$, and the lower row shows shoulder torque $-8\text{Nt-m} \sim +8\text{Nt-m}$ and torque $-15\text{Nt-m} \sim +10\text{Nt-m}$ for AB/AD flexion/extension respectively) larger than that in assistive mode (Fig. 15: the top row reveals similar angles as the top row of Fig. 14, however the lower row shows shoulder AB/AD torque $-8\text{Nt-m} \sim +6\text{Nt-m}$ and flexion/extension torque $-10\text{Nt-m} \sim +10\text{Nt-m}$). The results show the assistive mode helps the patients to achieve similar angular motions with less exerted torque. In addition, the patient consumes 131.72 joules in active mode and only 109.98 joules in assistive mode, proving that the former is more intensive.

C. Assist-as-needed

In assistive mode, a defined trajectory is used as the criterion with which to determine whether the rehabilitation robot indeed provides assistance. Fig. 16 and Fig. 17 show simultaneous elbow flexion/extension and shoulder internal/external rotations in assistive mode. The upper plot in Fig. 16 indicates the elbow

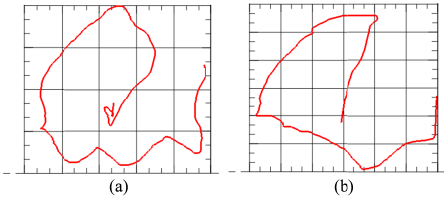


Fig. 13 End-point trajectory of window-cleaning game: (a) active mode and (b) assistive mode (trajectory starts from the far right and moves clockwise)

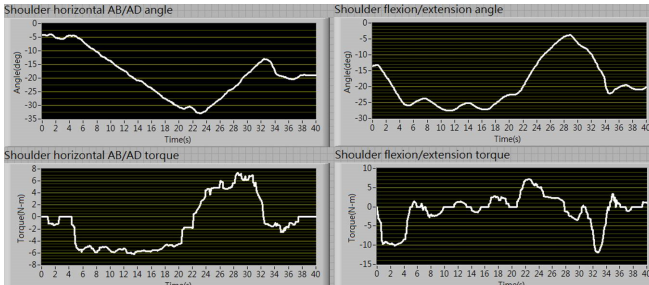


Fig. 14 Shoulder angle and torque of window-cleaning game in active mode

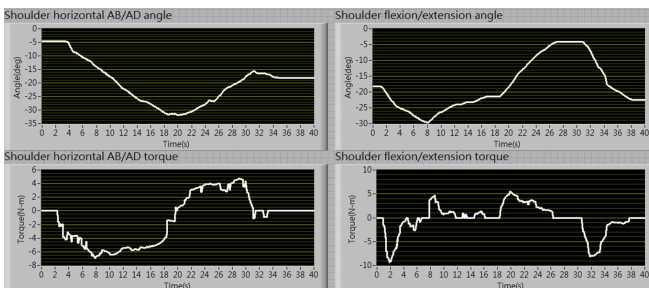


Fig. 15 Shoulder angle and torque of window-cleaning game in assistive mode

angle profile for elbow flexion/extension: the red curve is the defined trajectory, whereas the white curve is the measured trajectory. The lower plot in Fig. 16 indicates the torque exerted for elbow flexion/extension: the red curve is assistive torque from the robot arm, whereas the white curve is torque generated by the human subject. In (a) and (c), the measured angle of the human joint is unable to catch up with the desired trajectory; therefore, the robot provides assistive torque to support the subject. In (b) and (d), the measured angle of the human joint is capable of following or even exceeding the desired trajectory; therefore, the robot does not produce assistive torque to support the subject.

The upper plot in Fig. 17 illustrates the angle profile for the internal/external rotation of the shoulder: the red curve is the desired trajectory, whereas the white curve is the measured trajectory. The lower plot in Fig. 17 illustrates the joint torque for internal/external rotation of the shoulder: the red curve is the assistive torque from the robot arm, and the white curve is the torque generated by the human subject. In (a), (c), and (e), the measured angle profile of the human joint is unable to catch up with the desired trajectory; therefore, the robot provides assistive torque with which to support the subject. In (b), (d), and (f), the measured angle profile of the human joint is capable of following or even exceeding the desired trajectory; therefore, the robot does not provide assistive torque to support the subject. In brief, the robot arm assists the subject only when he/she is unable to finish the task, providing support only when the measured angle of the human joint is unable to follow the desired trajectory.

D. Clinical tests

To further validate the proposed system, clinical tests were conducted with six participants, one of which acted as a control. The demographics of the participants are listed in Table IV.

Table V presents the results of the Fugl-Meyer Test which evaluate motor recovery of stroke patients. The patient 1~5 belong to the experimental group, whereas the patient 6 is the control group. It should be noted that participants 3 and 4 suffered a stroke roughly one month before participating in the clinical tests and the scores of are much better than the patient who does not use robot assisted rehabilitation.

There are total twelve sessions of the robot rehabilitation. In each session, the participant was asked to move his/her shoulder from 0° to -45° back and forth twenty times as quickly as possible. Fig. 18 illustrates the shoulder joint angle and torque associated with the shoulder flexion/extension of participant 3. Fig. 18(a) illustrates the fifth session of therapy and Fig. 18(b) presents the ninth session. The lower graphs in each figure show the torque profile. The angle and torque in the time domain were transformed into the frequency domain, as illustrated in Fig. 19. It can be seen that the spectrum of fifth session is more scattered than ninth session due to the trembles and shakes of the patient's arm reduced through the therapy. Following assistive therapy, the participant was able to move the upper limb more smoothly and the movement was achieved in a shorter time (400 sec. vs. 430 sec.).

In another therapy, the patient was asked to move his/her elbow from 90° to 10° back and forth twelve times as quickly as

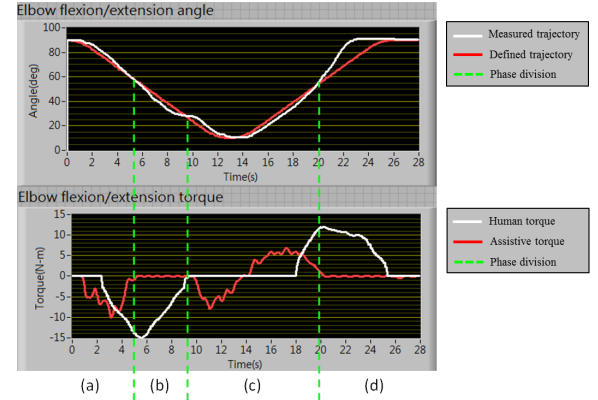


Fig. 16 Results of flexion/extension of the elbow in AAN assistive mode

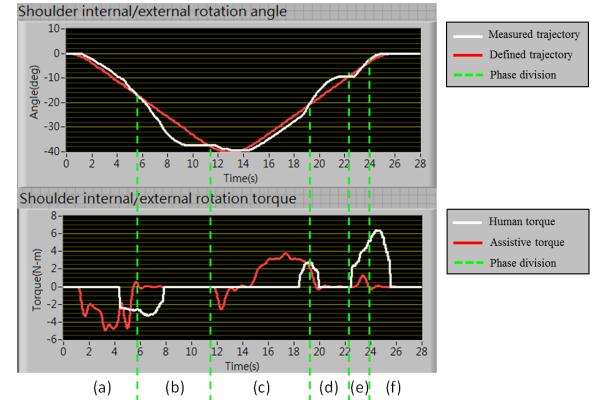


Fig. 17 Results of internal/external rotation of the shoulder in AAN assistive mode

Table IV. DEMOGRAPHICS

Subject	Gender	Age	Time since stroke (months)
Patient 1	Male	49	15
Patient 2	Female	58	4
Patient 3	Male	54	1
Patient 4	Male	83	1
Patient 5	Male	61	15
Patient 6	Male	46	8

Table V. FUGL-MEYER TEST

Subject	Joint	Before	After	Change
Patient 1	Shoulder/Elbow/Forearm	10	10	0
Patient 2	Shoulder/Elbow/Forearm	8	10	2
Patient 3	Shoulder/Elbow/Forearm	29	35	6
Patient 4	Shoulder/Elbow/Forearm	15	23	8
Patient 5	Shoulder/Elbow/Forearm	33	35	2
Patient 6	Shoulder/Elbow/Forearm	28	27	-1

possible. Fig. 20 presents the elbow angle and torque profiles for flexion/extension of the elbow by participant 4. Fig. 20(a) outlines the results of the fifth session of therapy; Fig. 20(b) presents the results of the ninth session. The smoothness of the motion is demonstrated by a transformation of the results into the frequency domain as demonstrated in Fig. 21. The point of total harmonic distortion (THD) is also useful in this regard, defined as the ratio of the sum of the powers of all harmonic components except the fundamental component to the power of the fundamental frequency: THD of the ninth session was 232.06×10^{-3} less than that of the fifth session (555.65×10^{-3}).

Table VI outlines the results of the Stroke Rehabilitation Assessment of Movement (STREAM), which is meant to enable physical therapists to quantitatively evaluate the motor

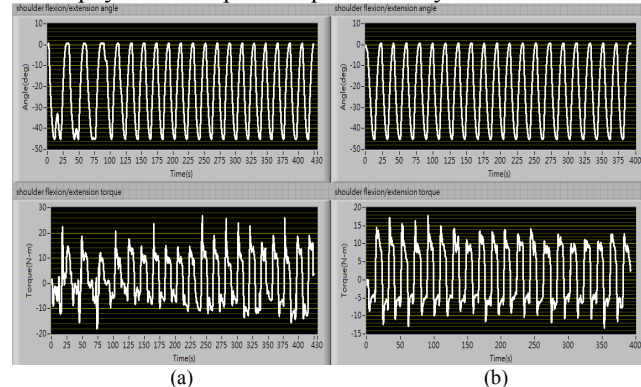


Fig. 18 Angle and torque of participant 3 in shoulder flexion\extension: (a) fifth session (b) ninth session

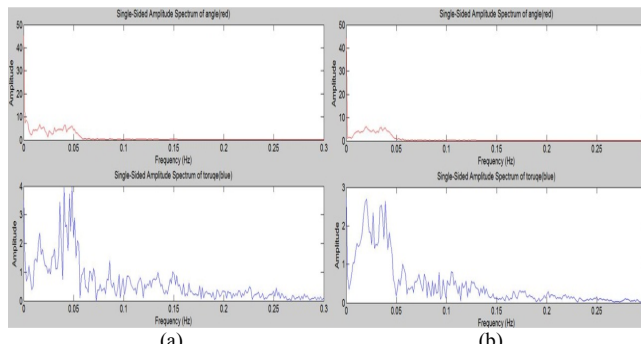


Fig. 19 Angle and torque of participant 3 in shoulder flexion\extension in frequency domain: (a) fifth session (b) ninth session

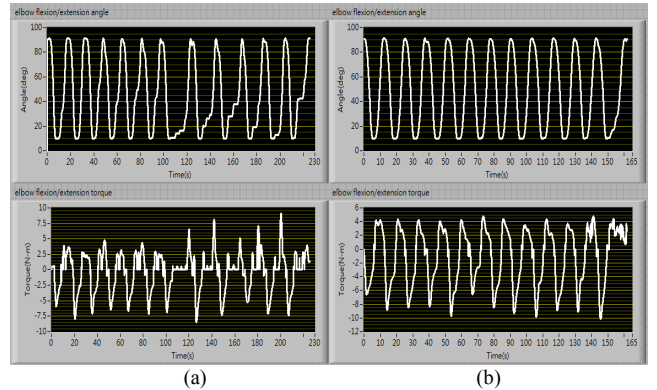


Fig. 20 Angle and torque of participant 4 in elbow flexion\extension: (a) fifth session (b) ninth session

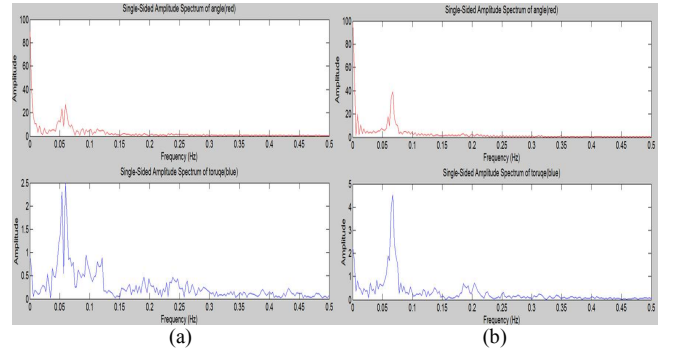


Fig. 21 Angle and torque of participant 4 in elbow flexion\extension in frequency domain: (a) fifth session (b) ninth session

functioning of stroke patients. STREAM includes three domains: upper limb, lower limb, and basic mobility. For the purposes of our experiment, this study focused on the upper-limb domain, in which the maximal score for each item is three points, totaling 20 points. Participants 3 and 5 showed no difference before and after treatment as their scores were already close to the maximum. Participant 1 suffered from a stroke 15 months prior to treatment, which meant that his window-period for brain recovery may have already passed.

Table VI. STREAM RESULTS BEFORE AND AFTER NTUH-ARM THERAPY

Subject	Before	After	Change
Patient 1	2	2	0
Patient 2	2	3	1
Patient 3	19	19	0
Patient 4	8	13	5
Patient 5	20	20	0
Patient 6	12	15	3

VI. DISCUSSION

The goal of this study is to integrate the exoskeleton upper-limb rehabilitation robot NTUH-ARM with the proposed assistive control strategies for stroke patients. Compared with the end-effector devices [6-8], the exoskeleton robot arms possess larger ROM and can control individual joint angles. To be more imitative of human arm's motion than other exoskeleton-type robots [10-16], the NTUH-ARM was designed as a 7-DOF robot arm.

The assistive control strategy proposed in this work is based on the human arm dynamics. With the forces measured by the F/T sensors and gravity compensation, an ideal human arm

acceleration trajectory can be obtained from human arm dynamics. The parameters of arm dynamics change with different subjects and the derivation from online measured forces can provide correct assistance for individuals. In the window-cleaning game, we compared the exerted torques in active and assistive modes (Fig. 14 and 15). Owing to the assistance, the patient in assistive mode can achieve similar angular motions with less exerted torque. Each joint's assistive gain can be adjusted independently.

The Assist-as-needed strategy is another assistive training mode. Under the AAN mode, the robot no longer needs to provide full support throughout the course of motion trajectory; whereas the robot can impel subjects to use their own muscular strengths while trying to keep up with the predefined motion trajectory. Though the AAN strategy has been studied in some researches [22,23], we adopted different method. First, we define smooth trajectories for joint angle, angular velocity, and acceleration. Then, the predefined joint angle trajectory is used as the basis and compared with human joint angle to determine the timing when the assistive torques are needed (Fig. 16, 17 and (24)). With this mechanism, the robot can give support to the subject only when his/her motion falls behind the predefined trajectory (Fig. 16-(a), (c) and Fig. 17-(a), (c), (e)). The Lyapunov stability analysis has been provided for this control strategy to ensure the theoretical correctness.

VII. CONCLUSION

This paper presents an assistive control system for a rehabilitation robot arm with 7-DOF deployed in the National Taiwan University Hospital-ARM (NTUH-ARM). By incorporating a human arm dynamic model and real-time measurements of human-exerted torque with two 6-axis F/T sensors, we were able to realize our goals of utilizing patient-cooperative control strategies in passive, active and assistive modes with gravity compensation for robot-aided stroke recovery. To verify the effectiveness of the proposed system, we first analyzed the stability of the closed loop system using Lyapunov theory, and then subjected the system to empirical testing. We also conducted clinical trials with 6 patients specifically testing the proposed AAN strategy. We obtained positive results for acute stroke patients in the clinical trials as well as in STREAM results obtained by physical therapists. A follow-up study is currently under way to determine whether such promising results can be obtained among patients whose stroke symptoms are less acute.

REFERENCES

- [1] American Heart Association: *Heart and Stroke Statistics Update* <http://www.Americanheart.org/statistics/stroke.htm> 2012.
- [2] G. Kwakkel, R. C. Wagenaar, T. W. Koelman, G. J. Lankhorst, and J. C. Koetsier, "Effects of intensity of rehabilitation after stroke" *Stroke*, pp. 1550-1556, 28 1997.
- [3] N. A. Bayona, J. Bitensky, K. Salter, and R. Teasell, "The role of task-specific training in rehabilitation therapies," *Top Stroke Rehabil*, vol. 12, pp. 58-65, Summer 2005.
- [4] C. Butefisch, H. Hummelsheim, P. Denzler, and K. H. Mauritz, "Repetitive training of isolated movements improves the outcome of motor rehabilitation of the centrally paretic hand," *J Neurol Sci*, vol. 130, pp. 59-68, May 1995.
- [5] N. Hogan, H. I. Krebs, B. Rohrer, J. J. Palazzolo, L. Dipietro, S. E. Fasoli, J. Stein, R. Hughes, W. R. Frontera, D. Lynch, and B. T. Volpe, "Motions or muscles? Some behavioral factors underlying robotic assistance of motor recovery," *J Rehabil Res Dev*, vol. 43, pp. 605-18, Aug-Sep 2006.
- [6] H. Krebs, M. Ferraro, S. Buerger, M. Newberry, A. Makiyama, M. Sandmann, D. Lynch, B. Volpe, and N. Hogan, "Rehabilitation robotics: pilot trial of a spatial extension for MIT-Manus," *Journal of NeuroEngineering and Rehabilitation*, vol. 1, p. 5, 2004.
- [7] P. S. Lum, C. G. Burgar, M. Van der Loos, P. C. Shor, M. Majmundar, and R. Yap, "MIME robotic device for upper-limb neurorehabilitation in subacute stroke subjects: A follow-up study," *J Rehabil Res Dev*, vol. 43, pp. 631-42, Aug-Sep 2006.
- [8] S. Coote, B. Murphy, W. Harwin, and E. Stokes, "The effect of the GENTLE/s robot-mediated therapy system on arm function after stroke," *Clin Rehabil*, vol. 22, pp. 395-405, May 2008.
- [9] Marc G. Carmichael, and Dikai Liu, "Estimating physical assistance need using a musculoskeletal model," *IEEE Trans. Biomedical Engineering*. DOI:10.1109/TBME.2013.2244889 (2013).
- [10] T. Nef, M. Mihelj, and R. Riener, "ARMin: a robot for patient-cooperative arm therapy," *Medical and Biological Engineering and Computing*, vol. 45, pp. 887-900, 2007.
- [11] M. Mihelj, T. Nef, and R. Riener, "ARMin II - 7 DoF rehabilitation robot: mechanics and kinematics," in *Proc. IEEE Int. Conf. Robotics and Automation*, 2007, pp. 4120-4125.
- [12] T. Nef, M. Guidali, and R. Riener, "ARMin III – arm therapy exoskeleton with an ergonomic shoulder actuation," *Appl Bionics Biomech*, vol. 6, pp. 127-142, 2009.
- [13] C. Carignan, J. Tang, and S. Roderick, "Development of an exoskeleton haptic interface for virtual task training," in *Proc. IEEE/RSJ int. conf. Intelligent Robots and Systems*, 2009, pp. 3697-3702.
- [14] P. Hyung-Soon, R. Yupeng, and Z. Li-Qun, "IntelliArm: An exoskeleton for diagnosis and treatment of patients with neurological impairments," in *Proc. IEEE RAS & EMBS Int. Conf. Biomedical Robotics and Biomechatronics*, 2008, pp. 109-114.
- [15] L. I. Lugo-Villeda, A. Frisoli, O. Sandoval-Gonzalez, M. A. Padilla, V. Parra-Vega, C. A. Avizzano, E. Ruffaldi, and M. Bergamasco, "Haptic guidance of Light-Exoskeleton for arm-rehabilitation tasks," in *Proc. IEEE Int. Symp. Robot and Human Interactive Communication*, 2009, pp. 903-908.
- [16] B.-C. Tsai, W.-W. Wang, L.-C. Hsu, L.-C. Fu, and J.-S. Lai, "An articulated rehabilitation robot for upper limb physiotherapy and training," in *Proc. IEEE/RSJ Int. Conf. Intelligent Robots and Systems*, 2010, pp. 1470-1475.
- [17] M. C. B. Moeslund T.B., Granum E., "Modelling the 3D pose of a human arm and the shoulder complex utilizing only two parameters," *Integrated Computer-Aided Engineering*, vol. 12, pp. 159-175, 2005.
- [18] G.-D. Lee, W.-W. Wang, K.-W. Lee, S.-Y. Lin, L.-C. Fu, J.-S. Lai, et al., "Arm exoskeleton rehabilitation robot with assistive system for patient after stroke," in *Proc. Int. Conf. Control, Automation and Systems*, 2012, pp.1943-1948.
- [19] W. H. Benno M. Nigg, *Biomechanics of the Musculo-Skeletal System* 3ed.: Wiley, John & Sons, Incorporated, 2007.
- [20] W. T. Dempster, *Space requirements of the seated operator*, 1955.
- [21] Li-Chun Hsu, Wei-Wen Wang, Guan-De Lee, Yi-Wen Liao, Li-Chen Fu, and Jin-Shin Lai, "A gravity compensation-based upper limb rehabilitation robot," in *Proc. American Control Conference*, 2012, pp. 4819-4824.
- [22] M. Uemura, K. Kanaoka, and S. Kawamura, "Power assist system for sinusoidal motion by passive element and impedance control," in *Robotics and Automation, 2006. ICRA 2006. Proceedings 2006 IEEE International Conference on*, 2006, pp. 3935-3940.
- [23] S. Rong, T. Kai-yu, H. Xiaoling, and L. Le, "Assistive Control System Using Continuous Myoelectric Signal in Robot-Aided Arm Training for Patients After Stroke," *Neural Systems and Rehabilitation Engineering, IEEE Transactions on*, vol. 16, pp. 371-379, 2008.
- [24] A. Duschau-Wicke, J. von Zitzewitz, A. Caprez, L. Lunenburger, and R. Riener, "Path Control: A Method for Patient-Cooperative Robot-Aided Gait Rehabilitation," *Neural Systems and Rehabilitation Engineering, IEEE Transactions on*, vol. 18, pp. 38-48, 2010.
- [25] J. L. Emken, J. E. Bobrow, and D. J. Reinkensmeyer, "Robotic movement training as an optimization problem: designing a controller that assists only as needed," in *Rehabilitation Robotics*, 2005. ICORR 2005. 9th International Conference on, 2005, pp. 307-312.